

On the alumina dust production in the winds of O-rich Asymptotic Giant Branch stars

F. Dell’Agli^{1,2}, D. A. García-Hernández^{3,4}, C. Rossi², P. Ventura¹,
M. Di Criscienzo¹, R. Schneider¹

¹*INAF – Osservatorio Astronomico di Roma, Via Frascati 33, 00040, Monte Porzio Catone (RM), Italy*

²*Dipartimento di Fisica, Università di Roma “La Sapienza”, P.le Aldo Moro 5, 00143, Roma, Italy*

³*Instituto de Astrofísica de Canarias, Vía Láctea s/n, E-38200 La Laguna, Tenerife, Spain*

⁴*Departamento de Astrofísica, Universidad de La Laguna (ULL), E-38206 La Laguna, Spain*

Accepted 2013 xx xx., Received 2013 xx xx; in original form 2013 xx xx

ABSTRACT

The O-rich Asymptotic Giant Branch (AGB) stars experience strong mass loss with efficient dust condensation and they are major sources of dust in the interstellar medium. Alumina dust (Al_2O_3) is an important dust component in O-rich circumstellar shells and it is expected to be fairly abundant in the winds of the more massive and O-rich AGB stars. By coupling AGB stellar nucleosynthesis and dust formation, we present a self-consistent exploration on the Al_2O_3 production in the winds of AGB stars with progenitor masses between ~ 3 and $7 M_\odot$ and metallicities in the range $0.0003 \leq Z \leq 0.018$. We find that Al_2O_3 particles form at radial distances from the centre between ~ 2 and $4 R_*$ (depending on metallicity), which is in agreement with recent interferometric observations of Galactic O-rich AGB stars. The mass of Al_2O_3 dust is found to scale almost linearly with metallicity, with solar metallicity AGBs producing the highest amount (about $10^{-3} M_\odot$) of alumina dust. The Al_2O_3 grain size decreases with decreasing metallicity (and initial stellar mass) and the maximum size of the Al_2O_3 grains is $\sim 0.075 \mu\text{m}$ for the solar metallicity models. Interestingly, the strong depletion of gaseous Al observed in the low-metallicity HBB AGB star HV 2576 seems to be consistent with the formation of Al_2O_3 dust as predicted by our models. We suggest that the content of Al may be used as a mass (and evolutionary stage) indicator in AGB stars experiencing HBB.

Key words: Stars: abundances; Stars: AGB and post-AGB; ISM: abundances, dust; astrochemistry; circumstellar matter; ISM: molecules

1 INTRODUCTION

During the Asymptotic Giant Branch (AGB) phase, stars of low- and intermediate-mass ($1M_\odot \leq M \leq 8M_\odot$) experience high mass-loss rates (Herwig 2005), thus an efficient dust condensation (Ferrarotti & Gail 2001, 2002, 2006) occurs in their circumstellar envelopes. In fact, they are one of the most important contributors of dust to the interstellar medium. We note that core-collapse supernovae (SNe) are also major producers of dust grains (Matsuura et al. 2011; Gomez et al. 2012; Tenorio-Tagle et al. 2013); indeed the study of the stellar source/s (e.g., AGB stars and/or SNe) for interstellar and presolar dust grains is a hot topic of extreme interest for the astrophysical community (Trigo-Rodríguez et al. 2009, Valiante et al. 2009, Gall et al. 2011).

AGB stars experience a series of periodic, thermally unstable, ignitions of the He shell, in what is commonly known as thermal pulse (TP) (Schwarzschild & Harm 1965, 1967).

The third dredge-up (TDU), occurring during the TP-AGB phase, may alter the surface chemical abundances in AGBs, favoring a gradual carbon enrichment of the external layers, until the originally O-rich star becomes C-rich ($\text{C/O} > 1$). The more massive ($> 3 - 4 M_\odot$) stars, however, may remain O-rich during the whole AGB evolution as a consequence of the activation of the hot bottom burning (HBB) process (see e.g., Blöcker & Schönberner 1991, Mazzitelli et al. 1999; García-Hernández et al. 2007a and references therein). Thus, the dominant chemistry of dust grains produced by AGB stars mainly depends on their progenitor masses and metallicities (Ventura et al. 2012a,b, 2014). Low mass AGBs ($M \leq 3M_\odot$) produce oxygen-rich dust as far as the surface C/O is below unity. However, this dust production is in limited quantities, given the low-mass loss rates experienced during these evolutionary phases. These stars are expected to form considerable amount of carbonaceous dust once the C/O ratio exceeds unity, because of the large

number of carbon molecules available and the higher mass-loss rate experienced towards the end of the AGB phase (Wachter et al. 2008). On the other hand, more massive AGBs - where HBB prevents the formation of carbon stars - produce oxygen-based dust (such as amorphous and crystalline silicates, Sylvester et al. 1999; García-Hernández et al. 2007b).

The dust condensation sequence as well as the most important molecules in the nucleation process are different for C- and O-rich AGB stars. The formation of dust grains in the winds of C-rich AGBs seems to be rather well established with several forms of carbon (e.g., small hydrocarbon molecules such as acetylene) believed to be the building blocks of more complex organic molecules and grains (Cherchneff & Cau 1999). However, the process of dust formation and grain growth in O-rich AGB stars is less clear (e.g., Woitke 2006; Norris et al. 2012; Zhao-Geisler et al. 2012) and needs further observational and theoretical efforts.

The spectral energy distributions (SEDs) observed in O-rich AGB stars can be reproduced with alumina (Al_2O_3) dust envelopes, amorphous silicates dust shells, or a mix of both species (e.g., Lorenz-Martins & Pompeia 2000; Maldoni et al. 2005). In addition, the $13\ \mu\text{m}$ dust emission feature generally observed in the spectra of O-rich AGBs is attributed to corundum (crystalline Al_2O_3) dust grains (Posch et al. 1999; Sloan 2003; DePew et al. 2006; Yang 2008; Takigawa et al. 2009; Zeidler et al. 2013; Jones et al. 2014). This shows that aluminium-based dust species represent a major dust component in O-rich circumstellar shells. Al_2O_3 dust grains - because of their high stability and transparency - have been suggested as good candidates to explain the dusty regions observed extremely close to the stellar surface (Woitke 2006; Norris et al. 2012; Zhao-Geisler et al. 2012). Furthermore, Infrared Space Observatory (ISO) spectra of Galactic bulge AGBs were found to display alumina dust component much stronger than silicates ones, suggesting Al_2O_3 grains as a likely starting point in O-rich dust condensation sequence (Blommaert et al. 2006). By following these earlier studies, Karovicova et al. (2013) have recently analysed the mid-IR multi-epoch interferometric observations of several O-rich AGB stars. Interestingly, their interferometric results indicate that Al_2O_3 grains condense very close to the stellar surface (at about 2 stellar radii which is much closer than warm silicate grains¹) and that they can be seed particles for the further O-based dust condensation.

The more massive and O-rich HBB AGB stars have been suggested as major alumina dust producers (Sedlmayr 1989; Gail & Sedlmayr 1998). The strong HBB experienced by these stars would favour a considerable increase in the Al content at the stellar surface because of the activation of the Mg-Al nucleosynthesis at the bottom of the convective envelope. Presolar alumina grains originated from AGB stars were found in primitive chondrites (Hutcheon et al. 1994, Choi et al. 1998, Nittler et al. 2008, Takigawa et al. 2014), which is direct evidence of alumina formation around AGB stars. In addition, an ^{26}Al excess is widely found in primitive

refractory materials (such as calcium and aluminium-rich inclusions; CAIs), and this ^{26}Al excess may be explained by pollution from a nearby massive AGB and/or super-AGB star during the Early Solar System (ESS) (see e.g., Trigo-Rodríguez et al. 2009; Lugaro et al. 2012, and references therein). Despite their broad astrophysical interest, a self-consistent investigation (i.e., by coupling AGB stellar nucleosynthesis and dust formation) on the production of Al_2O_3 in the surroundings of AGB stars is still lacking in the literature.

In the present work, we attempt to fill this gap, by investigating the formation of alumina dust in the winds of AGBs. We restrict our attention to O-rich stars, spanning the range of metallicities $3 \times 10^{-4} \leq Z \leq 0.018$. The paper is organized as follows: the details of stellar evolution modelling and the description of dust formation process in AGB winds are presented in Section 2; Section 3 is focused on the properties of the Al_2O_3 molecule and on the Mg-Al nucleosynthesis in HBB AGBs, which determines the change in the surface content of aluminium. The formation and growth of alumina dust grains is described in Section 4 together with a discussion on the uncertainties of the results, due in particular to the poor knowledge of the sticking coefficient; Section 5 presents a comparisons of our results with the observations available in the literature. Finally, Section 6 we draw the main conclusions of the present study.

2 THE MODEL

2.1 Stellar evolution models

We computed the stellar evolutionary sequences for different progenitor masses ($3M_{\odot} \leq M \leq 7M_{\odot}$) and metallicities ($3 \times 10^{-4} \leq Z \leq 0.018$, see below) by using the code ATON. We refer the reader to Ventura et al. (1998) and Ventura & D’Antona (2009) for a complete description of the numerical structure of the code and of the most recent updates, respectively. We report here only the physical inputs relevant for the present investigation.

The temperature gradient in regions unstable to convection was determined by the Full Spectrum of Turbulence (FST) model presented by Canuto & Mazzitelli (1991). This choice is crucial for the results obtained, because of the great impact of the convection model used on the description of the AGB evolution (Ventura & D’Antona 2005; García-Hernández et al. 2013), and, consequently, on the type of dust formed around massive AGBs (Ventura et al. 2012a,b, 2014).

Mass loss was modeled according to the treatment discussed in Blöcker (1995). This choice is extremely relevant in order to determine the amount of dust formed, because, as we will discuss in the following Section, the mass-loss rate determines the density of the gas in the wind and thus the number of gas molecules potentially able to condense into dust.

The chemical mixtures used to define the initial composition of the models were chosen following Grevesse & Sauval (1998). For the $Z = 3 \times 10^{-4}$ case we used an α -enhancement $[\alpha/\text{Fe}] = +0.4$, for the metallicities $Z = 4 \times 10^{-3}$ and $Z = 8 \times 10^{-3}$ we adopted $[\alpha/\text{Fe}] = +0.2$, whereas for $Z = 0.018$ we used a solar-scaled mixture.

¹ Note that this is supported by theoretical thermodynamic calculations that show that Al_2O_3 condenses at higher temperatures ($\sim 1400\ \text{K}$) than several types of silicates ($\sim 1100\ \text{K}$) (e.g., Tielens et al. 1998)

2.2 Wind structure and dust formation

We model the structure of the wind by following the schematisation described in the series of papers by Ferrarotti & Gail (2001, 2002, 2006). We summarize here the main aspects of this model.

Based on the results from stellar evolution modelling, (i.e., the temporal evolution of mass, M , luminosity, L , effective temperature, T_{eff} , and mass-loss rate of the star, \dot{M}), and assuming an isotropically expanding wind, we integrate a set of equations to determine the radial distribution of velocity (v), temperature (T), density (ρ), and opacity (k) of gas molecules.

From the equation of momentum conservation we determine the radial velocity gradient of the wind (in the following, we indicate with r the distance from the centre of the star):

$$v \frac{dv}{dr} = -\frac{GM}{r^2}(1 - \Gamma). \quad (1)$$

Γ is the ratio between the radiation pressure on the dust grains and the gravitational pull:

$$\Gamma = \frac{kL}{4\pi cGM} \quad (2)$$

and k is the flux-averaged extinction coefficient

$$k = k_{gas} + \sum_i f_i k_i. \quad (3)$$

Eq. 3 contains the gas contribution $k_{gas} = 10^{-8} \rho^{2/3} T^3$ (Bell & Lin 1994), and the sum of the absorption and scattering coefficients extended to all the dust species considered.

The f_i 's in Eq. 3 are the degrees of condensation of the key elements for each dust species, whereas the k_i 's are the corresponding extinction coefficients.

When k increases, owing to dust formation, and Γ becomes greater than unity, the wind is accelerated by the radiation pressure. In the equation describing the radial variation of velocity we neglect pressure forces, because they are negligible compared to gravity. This assumption holds in the present treatment, because we do not consider any shock structure of the outflow.

Starting from mass conservation, we can write the density of the wind as:

$$\dot{M} = 4\pi r^2 \rho v, \quad (4)$$

The temperature stratification is determined assuming the grey atmosphere approximation:

$$T^4 = \frac{1}{2} T_{eff}^4 \left[1 - \sqrt{1 - \frac{R_*^2}{r^2}} + \frac{3}{2} \tau \right], \quad (5)$$

where R_* is the stellar radius. The optical depth, τ , is found via the differential equation:

$$\frac{d\tau}{dr} = -\rho k \frac{R_*^2}{r^2}. \quad (6)$$

In order to close the system of equations we need to find

the f_i 's, which, in turn, depend on the type and the amount of dust formed. In the present investigation, focused on the winds of O-rich AGB stars, we account for the formation of alumina dust, solid iron and Mg-silicates (forsterite, enstatite and quartz). For alumina dust and Mg-silicates we consider the amorphous state since the physical conditions present in stellar outflows are more favourable to condensation as amorphous material than crystallized form. Clearly, we cannot rule out that part of the dust is present in crystalline state (e.g. corundum or crystalline Al_2O_3), which would imply the appearance of strong and specific solid-state features in the mid-infrared spectra of O-rich AGB stars; e.g. the spectral features of corundum at $13 \mu m$ and of crystalline silicates at $\sim 10 \mu m$ as well as at $20 \mu m$.

We describe the dust growth process by vapour deposition on the surface of some pre-formed seed nuclei, assumed to be nanometer sized spheres. Each dust species has a key element, which is the least abundant among the elements necessary to form the corresponding dust aggregate. The growth of the size of dust grains (a) of a given species i is determined via a competition between a production term (J_i^{gr}), associated to the deposition of new i molecules on already formed grains, and a destruction factor (J_i^{dec}), proportional to the vapor pressure of the key species i on the solid state:

$$\frac{da_i}{dt} = V_{0,i} \left(J_i^{gr} - J_i^{dec} \right), \quad (7)$$

where $V_{0,i}$ is the volume of the nominal molecule in the solid. Both J_i^{gr} and J_i^{dec} are directly dependent on the value of the sticking coefficient, α_i , which varies according to the species considered. From the dust grains size (a_i) we calculate the degree of condensation of the key element into solid state (f_i) via the expression:

$$f_i = \frac{4\pi(a_i^3 - a_{0,i}^3) \epsilon_d}{3V_{0,i} \epsilon_k} \quad (8)$$

where the initial dust grains size ($a_{0,i}$) is assumed to be equal to a midrange value of $0.01 \mu m$, ϵ_k is the number density of the key elements in the wind, normalized to the hydrogen density, and the normalized density of the seed nuclei ϵ_d is assumed to be 10^{-13} (Knapp 1985).

Finally, to determine the mass M_i of the dust species i produced during the entire AGB phase, we use the equation:

$$\frac{dM_i}{dt} = \dot{M} X_k \frac{A_i}{A_k} f_i. \quad (9)$$

where X_k and A_k are the surface mass fraction and molecular weight of the key-element, and A_i is the molecular weight of the dust species considered.

3 ALUMINA DUST IN THE WINDS OF AGBS

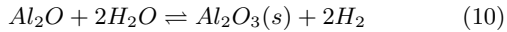
The thermodynamical conditions of O-rich AGB winds are favorable to form various types of oxygen-based dust, including alumina dust. This is because these stars evolve at large luminosities, they lose mass at very high rates and their envelopes are extremely cool; thus, the dust formation region

is close to the stellar surface, where the densities are sufficiently large to allow condensation into dust of considerable amounts of gas molecules.

In this section, we discuss the main properties of Al_2O_3 to understand its condensation process and the impact on the overall dust production in the winds of O-rich AGB stars.

3.1 Al_2O_3 properties

The reaction leading to the formation of Al_2O_3 is



where Al_2O and H_2O are the most abundant Al- and O-based molecules not bound in solid state². Clearly, aluminium is the key-element for the production of this dust specie.

To analyze the formation of alumina dust relatively to Mg-silicates, we show in Fig. 1 the stability lines of Al_2O_3 , forsterite (Mg_2SiO_4), quartz (SiO_2) and iron, in the P-T plane. We clearly see that alumina, owing to an extremely high energy of formation (Sharp & Huebner 1990), is by far the most stable compound, allowing the formation of Al_2O_3 grains at temperature as high as ~ 1500 K. In the same Figure, we also show the structure of the winds surrounding models of a $6 M_\odot$ initial mass at different metallicities. The plot refers to the phase of highest luminosity, with the maximum strength of the dust formation process, after $\sim 1 M_\odot$ was lost by the star.

The refraction index used for the computation of the extinction coefficients for alumina dust are taken from Koike et al. (1995), who present optical constants for crystalline Al_2O_3 . A comparison with the more recent results from Begemann (1997), who consider the amorphous case, indicates no meaningful differences in the Al_2O_3 production. This adds more robustness to our results.

However, concerning the amorphous or crystalline nature of the Al_2O_3 formed, any prediction is made difficult by the fact that the threshold temperature above which the crystalline component is dominant (~ 1440 K Levin & Brandon 1998) is within the range of temperatures at which the condensation process takes place (1200–1500 K). The high abundance of amorphous alumina in the circumstellar envelopes of many O-rich AGB stars confirms the presence of the amorphous component, but the details of the relative distribution of the two phases of Al_2O_3 is beyond the scopes and the possibilities of the present analysis. From our analysis, however, we cannot draw any conclusion on the amorphous or crystalline nature of the Al_2O_3 formed.

The rate at which Al_2O_3 grains grow in the expanding winds of AGBs is unfortunately made uncertain by the

² Indeed use of eq. 10 assumes that all the gaseous Al available is locked into Al_2O molecules. Actually AlOH is also expected to be present in not negligible quantities in AGB winds (Sharp & Huebner 1990), which would require the treatment of the alternative channel for the formation of Al_2O_3 , i.e. $2\text{AlOH} + \text{H}_2\text{O} \rightleftharpoons \text{Al}_2\text{O}_3(s) + 2\text{H}_2$. The results we obtain, neglecting the Al locked into AlOH , might partly overestimate the amount of Al_2O_3 formed.

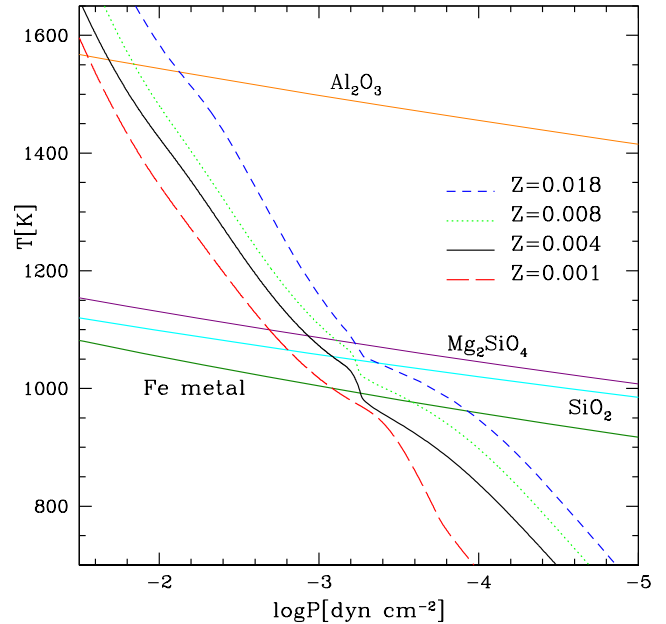


Figure 1. Thermodynamic stratification in the P-T plane of the winds of $6 M_\odot$ models in the phase of maximum luminosity when $\sim 1 M_\odot$ was lost from the envelope. The different lines correspond to the metallicities $Z = 0.001$ (red dashed-dotted line), $Z = 0.004$ (black solid line), $Z = 0.008$ (green dotted line), and $Z = 0.018$ (blue dashed line). The surface mass fraction of (O, Mg, Al, Si) for the models shown are: (6.95×10^{-3} , 7.2×10^{-4} , 6.5×10^{-5} , 7.9×10^{-4}) for $Z=0.018$, (2.97×10^{-3} , 4.2×10^{-4} , 2.7×10^{-5} , 4.0×10^{-4}) for $Z=0.008$, (1.29×10^{-3} , 2.1×10^{-4} , 1.9×10^{-5} , 2.0×10^{-4}) for $Z=0.004$ and (1.64×10^{-4} , 4.8×10^{-5} , 1.3×10^{-5} , 5.6×10^{-5}) for $Z=0.001$. We also show the stability curves in the pressure-temperature (P-T) plane for Al_2O_3 (orange), Mg_2SiO_4 (purple), SiO_2 (cyan) and iron (dark green).

poorly known sticking coefficient. To date, the only robust measurement, limited to the crystalline form, indicates a value for the α_{al} smaller than 0.1 (Takigawa et al. 2012). In analogy with the amorphous Mg-silicates, we thus assume as reference value $\alpha_{al}=0.1$. However, we investigate the sensitivity of our results to α_{al} in Section 4.2, where we explore different values of the sticking coefficient.

3.2 Hot bottom burning in massive AGBs and the activation of the Mg-Al chain

As we have mentioned above, stars of initial mass above $\sim 3 M_\odot$ (this limit depends also on the convection model adopted, see Renzini & Voli 1981, Ventura & D’Antona 2005, García-Hernández et al. 2013) experience hot bottom burning. The bottom of the convective envelope becomes sufficiently hot to activate an advanced proton-capture nucleosynthesis, with the consequent modification of the surface chemistry. The temperature at the bottom of the convective envelope T_{bce} is the key quantity in determining the extent of the nucleosynthesis experienced.

T_{bce} generally increases with core mass, and is higher for lower stellar metallicities model (Ventura et al. 2013). When T_{bce} reaches ~ 30 MK, lithium production via the

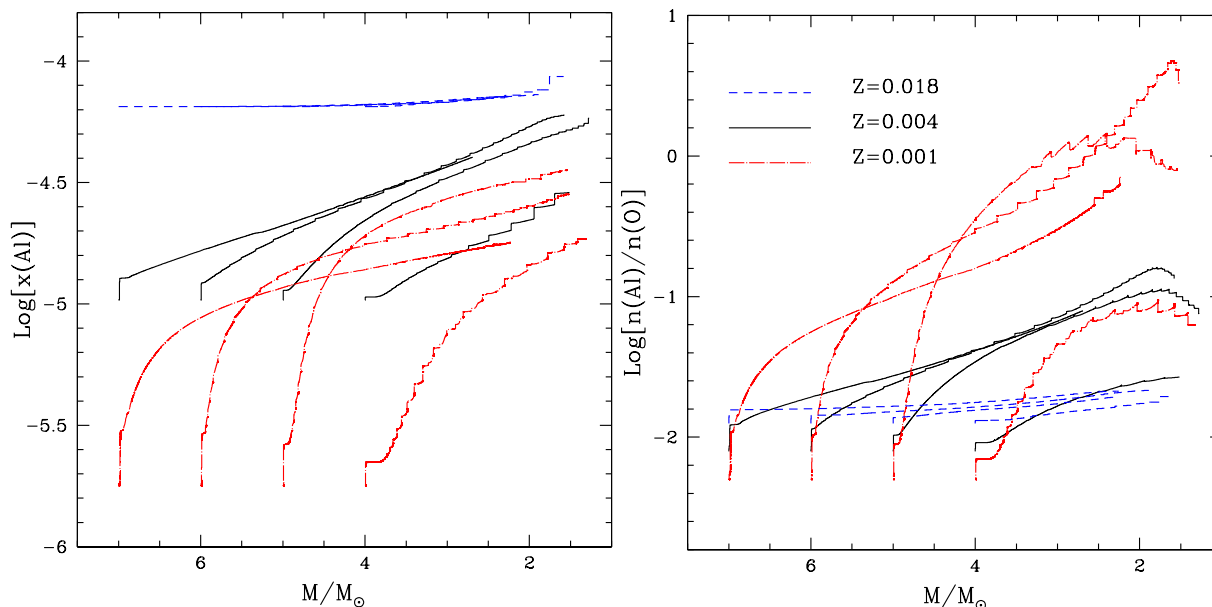


Figure 2. The surface mass fraction abundance of Al (left panel) and the number density ratio of Al and O (right panel) as a function of the current mass of the star. The predictions for models of 4, 5, 6, and 7 M_{\odot} at $Z = 0.001$ (red dashed-dotted line), 0.004 (black solid line) and 0.018 (blue dashed line) are displayed. Note that stellar mass decreases during the evolution in the AGB and takes place from left to right.

Cameron–Fowler mechanism and carbon destruction via p-capture are achieved. At temperatures of the order of ~ 70 – 80 MK, oxygen undergoes proton fusion and is destroyed. When T_{bce} exceeds ~ 80 MK, the innermost regions of the envelope become site of a series of proton capture reactions involving the isotopes of magnesium, that eventually lead to the production of aluminium (Ventura, Carini & D’Antona 2011). Because the initial magnesium is much larger than aluminium, even a small depletion of the surface magnesium is sufficient to induce a considerable increase in the surface Al-content.

Ignition of the Mg-Al nucleosynthesis is crucial for the discussion concerning the production of Al_2O_3 , because in the vast majority of cases aluminium drives the formation process for this species.

The left panel of Figure 2 shows the variation of the surface Al-content of models of different mass, for three of the four metallicities investigated in this work (for clarity reasons, in the figure we omit $Z=0.008$). The choice of the logarithmic scale allows to appreciate the extent of the Al-increase.

In agreement with the previous discussion, we note the following:

(i) The percentage increase in the surface aluminium is higher in models of lower metallicity. While in the $Z=10^{-3}$ case the surface Al is increased by a factor ~ 10 – 20 , in the $Z=8 \times 10^{-3}$ the increase is limited to a factor ~ 2 . No change is found in the solar case.

(ii) Models of higher mass generally produce more aluminium, because they experience a stronger HBB. However, the most massive models of metallicity $Z=10^{-3}$ and $Z=4 \times 10^{-3}$ eject gas less enriched in aluminium

than their smaller mass counterparts; this is due to the strong mass loss experienced, so that the envelope is completely lost before a great production of aluminium occurs (Ventura, Carini & D’Antona 2011).

Figure 2 (right panel) shows the variation of Al/O in the same models shown in the left panel. Al/O increases with time due to the simultaneous production of aluminium and destruction of oxygen, but remains below unity in all cases, with the only exception of the latest evolutionary phases of the more massive models at $Z=10^{-3}$: only in these latter models the destruction of the surface oxygen eventually leads to the condition $\text{Al}/\text{O} > 1$, which makes oxygen the key element in the production of Al_2O_3 . Therefore, we may safely assume in the following analysis that aluminium is the key-element for the formation of alumina dust.

4 ALUMINA DUST PRODUCTION

Here, we discuss dust formation in AGB models of metallicities $3 \times 10^{-4} \leq Z \leq 0.018$. Because Al_2O_3 forms only in O-rich environments, we restrict the present analysis to stars of mass above $3M_{\odot}$. Models with $Z=4 \times 10^{-3}$ and $Z=0.018$ have been calculated specifically for this paper. Models with $Z=3 \times 10^{-4}$, 10^{-3} , 8×10^{-3} were published in previous investigations by our group (Ventura et al. 2012a,b; Di Criscienzo et al. 2013; Ventura et al. 2014). However, the dust formation modelling was repeated here, because Al_2O_3 formation was ignored in our previous works. In addition, we may disregard the $Z=3 \times 10^{-4}$ models from our investigation - dust production in O-rich AGB stars of this metallicity is too low to drive the wind, owing to the extremely low abun-

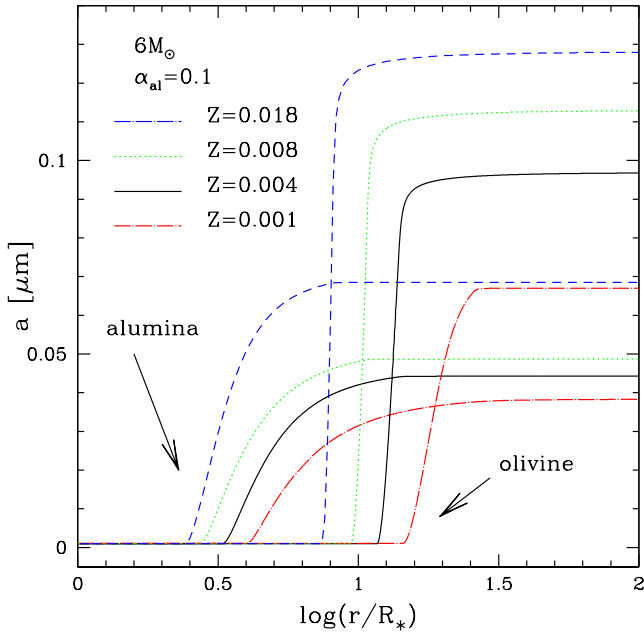


Figure 3. Size of the Al_2O_3 and forsterite dust grains as a function of the distance from the centre of the star, for the same models of Fig. 1. Note that we have assumed the sticking coefficient $\alpha_{al} = 0.1$ in the simulations.

dances of silicon and aluminium (see Di Criscienzo et al. (2013)).

4.1 The growth of Al_2O_3 grains

Figure 3 shows the size of Al_2O_3 and Mg-silicates (here represented by forsterite dust) grains at different distances from the centre of the star, for the same models of Fig. 1. Iron grains form in minor quantities, in even more external regions, compared to Mg-silicates. They are omitted, for clarity reasons, in the present and the following figures. These profiles refer to an interpulse phase during the AGB evolution, when the dust production is at the highest rate; this occurs in all the cases shown in Figure 3 after $\sim 1M_\odot$ was lost from the star.

The exact location of the condensation zone is mainly determined by the effective temperature (T_{eff}) of the star (see eq. 5). Therefore, the trend with metallicity is straightforward: in solar metallicity models, owing to their lower T_{eff} , the growth of Al_2O_3 particles begins at $\sim 2R_*$ from the center of the star (blue dashed track in Fig.3), while at $Z = 0.001$ the Al_2O_3 condensation zone is in more external circumstellar regions, at $\sim 4R_*$ (red dotted-dashed line). On the other hand, a change in the initial mass of the star does not strongly affect these results because models with the same Z and different masses evolve at approximately the same T_{eff} .

The condensation of Al_2O_3 does not inhibit (or severely influence) the formation of Mg-silicates, owing to its large transparency: the acceleration of the wind via radiation pressure starts further the formation of the alumina dust, where

Mg-silicates begins to grow. Although, the formation of alumina dust determines a slight increase in the opacity, in turn, leads to a steeper gradient of the optical depth (τ , see eq. 6). Because of the boundary condition that τ vanishes at infinity, this can be accomplished only via an increase of τ in the regions internal to the Al_2O_3 formation layer. The higher τ favours an increase of the temperatures (see eq. 5). Therefore, in the present models, forsterite dust grains begin to grow in more external regions, at a distance of $\sim 10R_*$ from the star’s centre, where the densities are smaller and the amount of forsterite dust produced is thus consequently slightly reduced. This is accompanied by a larger production of enstatite and quartz dust. The total effect on the amount of dust product it will be discussed in Section 4.3.

The left and middle panels of Figure 4 show the variation during the AGB phase of the size of forsterite and Al_2O_3 grains, respectively. The different lines correspond to models of initial masses 4 and 6 M_\odot of several metallicities (other masses were omitted for clarity reasons).

The two panels of Fig. 5 show, for the same models, the variation of f_{al} (see Eq. 8), the fraction of aluminium condensed into dust.

The results obtained can be synthesized as follows:

(i) The size reached by forsterite and Al_2O_3 grains increases with metallicity, owing to the larger silicon and aluminium mass fractions in the surface layers of higher- Z models.

(ii) For a given Z , the dust grain size increases with the progenitor mass. This is because more massive stars experience a stronger HBB, and thus they evolve at higher luminosities and experience higher mass-loss rates.

(iii) The grain size evolution of forsterite and Al_2O_3 dust during the AGB phase is rather different. The maximum size of forsterite particles is reached when less than half of the envelope mass is lost. The dimension of the forsterite grains depends on metallicity, ranging from $\sim 0.07\mu\text{m}$ for $Z = 10^{-3}$, to $0.13\mu\text{m}$ for solar chemistry. Conversely, the size of Al_2O_3 grains increases during almost the whole AGB evolution. The decrease in the forsterite grain size is due to the drop in the total luminosity (and hence of the mass-loss rate) when the envelope mass is consumed. In the case of alumina dust, this effect is counterbalanced by the gradual increase in the surface Al content, favored by the activation of the Mg-Al nucleosynthesis. This is particularly important in massive, metal-poor AGB models (see left panel of Figure 2).

(iv) Solar metallicity models behave somewhat differently from their lower Z counterparts: the Al_2O_3 grain size attains the maximum values of $a_{al} \sim 0.075\mu\text{m}$ since the early AGB phases. For models of subsolar chemistry, a_{al} gradually increases as the star evolves, until a maximum value of $0.05 - 0.06\mu\text{m}$ (slightly dependent on Z) is reached in the more massive AGBs (see central panel of Fig.4). The alumina dust grains of the largest size are thus expected to form in the circumstellar shells of massive AGBs of solar metallicity, with $a_{al} \sim 0.07 - 0.08\mu\text{m}$.

(v) A high percentage of gaseous aluminium condenses into Al_2O_3 (almost $\sim 90\%$ in the higher mass AGB models, see left panel of Figure 5). We note that the evolution of f_{al} does not closely follow that of a_{al} (the Al_2O_3 dust grain size)

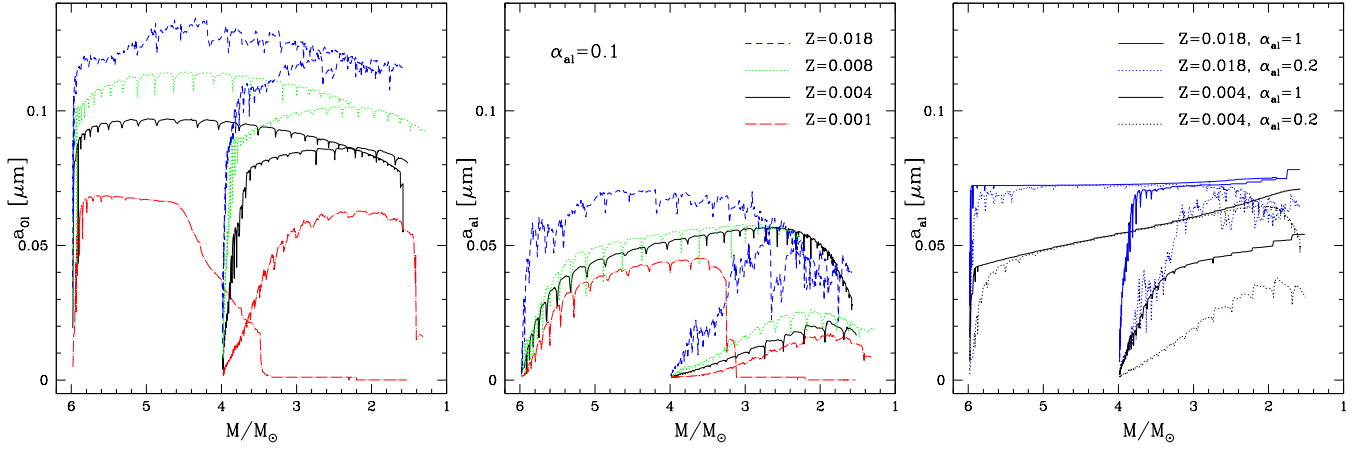


Figure 4. Evolution as a function of the total mass of the star of the forsterite (left panel) and Al_2O_3 (middle panel) dust grain sizes for models with progenitor masses of 4 and $6 M_\odot$ at $Z = 0.001$ (red dashed-dotted line), 0.004 (black solid line), 0.008 (green dotted line), and 0.018 (blue dashed line), assuming $\alpha_{al} = 0.1$. In the right panel we display the Al_2O_3 dust grain size versus the evolution of the stellar mass for models of 4 and $6 M_\odot$ models, at $Z = 0.004$ (black) and $Z = 0.018$ (blue), and by assuming two different values of the sticking coefficient - $\alpha_{al} = 0.2$ and 1 (dotted and solid lines, respectively).

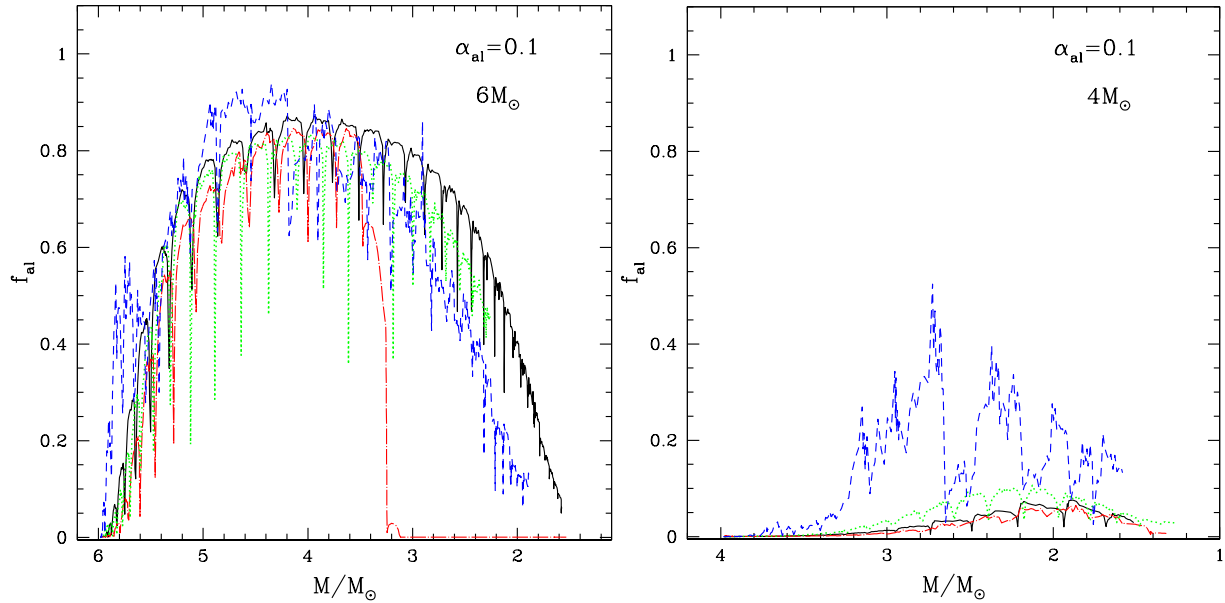


Figure 5. Evolution of the aluminium fraction condensed in Al_2O_3 (f_{al}) as a function of the evolution of the total mass by assuming $\alpha_{al} = 0.1$. We consider $6 M_\odot$ (left panel) and $4 M_\odot$ (right panel) initial mass model, at $Z = 0.001$ (red dashed-dotted line), $Z = 0.004$ (black solid line), $Z = 0.008$ (green dotted line), and $Z = 0.018$ (blue dashed line).

owing to the increase in the surface aluminium abundance (see Eq. 8).

(vi) Although Al_2O_3 dust grains form in more internal circumstellar regions and a high fraction of aluminium is condensed into dust, the size of the forsterite grains is still larger than that of Al_2O_3 . This is because the amount of silicon available is always much larger than aluminium.

The results given in points (i) (iii) and (iv) above are partly dependent on the choice of the initial density of seed

grains, ϵ_d . To understand how critical the choice of ϵ_d is, we run some simulations where ϵ_d was increased/decreased by a factor 10. The results in terms of the size reached by the grains of the various species of dust showed up only a modest dependence on ϵ_d , with a maximum variation by a factor 2 for a 1 dex variation of ϵ_d . The reason for this is that, based on Eq.8, the fraction f of the key-species condensed into dust goes as $\sim a^3 \epsilon_d$. Because the number of gaseous molecules available (that determines the growth rate of the

dust grains) depends critically on f , ($n \sim (1 - f)$), the effect of increasing/decreasing ϵ_d is partly counterbalanced by the same decrease/increase in a^3 . Note that a linear relation between ϵ_d and Z was invoked to account for the larger availability of the seed nuclei in more metal-rich environments (Nanni et al. 2013). Based on the arguments given above, such a scaling relation would reduce the difference in the size of Mg-silicates and alumina dust grains formed around models of different metallicity and would leave the initial mass of the star as the dominant factor determining the dimension of the particles formed.

4.2 The role of the sticking coefficient

Given the poor knowledge of the Al_2O_3 sticking coefficient (α_{al}) we discuss how the results presented in the previous sections depend on the choice of α_{al} , by exploring different values until $\alpha_{al}=1$.

We focus on the $4M_\odot$ and $6M_\odot$ models of metallicity $Z = 4 \times 10^{-3}$ and $Z = 0.018$. The evolution of the Al_2O_3 dust grain sizes obtained when using $\alpha_{al} = 0.2$ and $\alpha_{al} = 1$ are shown in the right panel of Figure 4, while the corresponding evolution of the fraction of aluminium condensed into Al_2O_3 is displayed in Figure 6.

As expected, adopting a larger α_{al} increases the Al_2O_3 grain size. However, in the $6M_\odot$ models of both metallicities α_{al} is almost independent of α_{al} : this is because f_{al} attains very large values, close to unity, even for $\alpha_{al} = 0.1$ (see left panel of Figure 5). Under these conditions, a further increase in α_{al} hardly leads to a further growth of the Al_2O_3 particles, which would be possible only if a considerable increase in the surface Al occurred.

Lower mass models behave somewhat differently. Unlike their more massive counterparts, for both the cases $Z = 4 \times 10^{-3}$ and $Z = 0.018$ we note a higher sensitivity to α_{al} . This stems from the fact that the saturation conditions are never reached, with f_{al} evolving below ~ 0.5 for $\alpha_{al} = 0.1$ (see right panel of Figure 5). Indeed, the right panel of Figure 6 shows that saturation in the $4M_\odot$ case is only reached for $\alpha_{al} = 1$. Note that for this mass, the maximum size reached by the Al_2O_3 grains - in the $\alpha_{al} = 1$ case for the two metallicities mentioned above - is $a_{al} \sim 0.075 \mu\text{m}$, which adds more robustness to the conclusions given in the previous subsection.

In case of an extremely small value of α_{al} ($= 0.01$) the growth of Al_2O_3 grains is severely inhibited. In the most massive models, suffering the strongest HBB, this would reflect in a decrease in the size of Al_2O_3 particles by a factor $\sim 2 - 3$. In the M-stars of smaller mass, such a small α_{al} would strongly suppress the formation of Al_2O_3 , whose grains would hardly exceed nanometer size dimensions.

4.3 Al_2O_3 mass production

The overall mass production of alumina dust is calculated by means of equation 9. In the left panel of Figure 7, we show the total mass of Al_2O_3 produced (M_{al}) during the whole AGB phase for different metallicities as a function of the initial mass of the star (M), assuming $\alpha_{al} = 0.1$.

The largest amount of alumina dust is produced by solar metallicity AGBs. M_{al} is strongly dependent on M , ranging

from $10^{-5}M_\odot$ for $M = 3M_\odot$, to $10^{-3}M_\odot$ for $M = 7M_\odot$. This trend with the mass of the star is found also for the other metallicities; M_{al} scales approximately linearly with Z .

To have an idea of the uncertainties associated with the choice of the sticking coefficient, we compare the results obtained with $\alpha_{al} = 0.1$ with those for $\alpha_{al} = 1$ (right panel of Fig. 7). In the latter case, the trend of M_{al} with the stellar mass is much flatter. This is because the saturation conditions are reached even for the lowest mass models experiencing HBB. In this case, the mass of alumina dust produced becomes practically independent of M , and scales approximately linearly with metallicity.

The comparison with the results by Ventura et al. (2012a,b), where formation of Al_2O_3 was not considered, allows to quantify the effects on the amount of Mg-silicates formed.

The total mass of dust produced, M_d , increases when the formation of Al_2O_3 is taken into account. For the more massive AGBs, M_d increases by $\sim 6 - 7\%$, while the amount of Mg-silicates formed, M_{sil} , decreases by $\sim 5\%$. For stars of lower mass no meaningful differences are found among the two cases, owing to the small quantities of alumina dust formed.

The differences introduced by considering the formation of Al_2O_3 are larger in the case $\alpha_{al} = 1$, because the condensation process is more efficient. In the massive AGBs domain the difference is purely quantitative, the total mass formed being increased by $\sim 15\%$. Unlike the standard case, for $M \sim 3 - 4M_\odot$, $\sim 20\%$ of dust is under the form of Al_2O_3 : neglecting the formation of alumina dust would underestimate considerably the overall amount of dust formed.

The reliability of the results obtained in terms of mass of dust M_d produced is partly affected by the intrinsic indeterminism in the choice of the density of seed particles, ϵ_d . However, as found for the dimension reached by the grains of the various species, the sensitivity of M_d on ϵ_d is modest, with a total variation below $\sim 50\%$ for a variation of one order of magnitude (see eq.9 and the discussion at the end of section 4.1).

Very recently, Nanni et al. (2013) presented models of dust formation around AGB stars, including also Al_2O_3 production, at three metallicities ($Z = 0.001, 0.008, \text{ and } 0.02$) and assuming $\alpha_{al} = 1$. Their models show no Al_2O_3 production at the lowest metallicity of 0.001 and for progenitor masses below $5 M_\odot$ at higher metallicity (see right panel of Figure 7). This is in contrast with our models where we find, at least for the more massive ($> 5 M_\odot$) stars, that a significant amount of Al_2O_3 is also formed at very low metallicity ($Z = 0.001$). This difference is mainly due to the different treatment of convection in the stellar evolution model. As we have mentioned above, the FST description of convection used in our models implies strong HBB conditions, which are not found in the Nanni et al. (2013) AGB models. At the higher metallicities, $Z = 0.008$ and $Z = 0.02$, and for initial masses $\geq 5 M_\odot$, the Al_2O_3 production found by Nanni et al. (2013) is comparable to ours. Much larger differences are seen for the lower masses ($< 5 M_\odot$), in which the mass of Al_2O_3 dust formed is always below $10^{-4} M_\odot$ in the Nanni et al. (2013) models; on the contrary, our AGB models predict Al_2O_3 production between 10^{-4} and $10^{-3} M_\odot$. This difference is again due to the much softer HBB

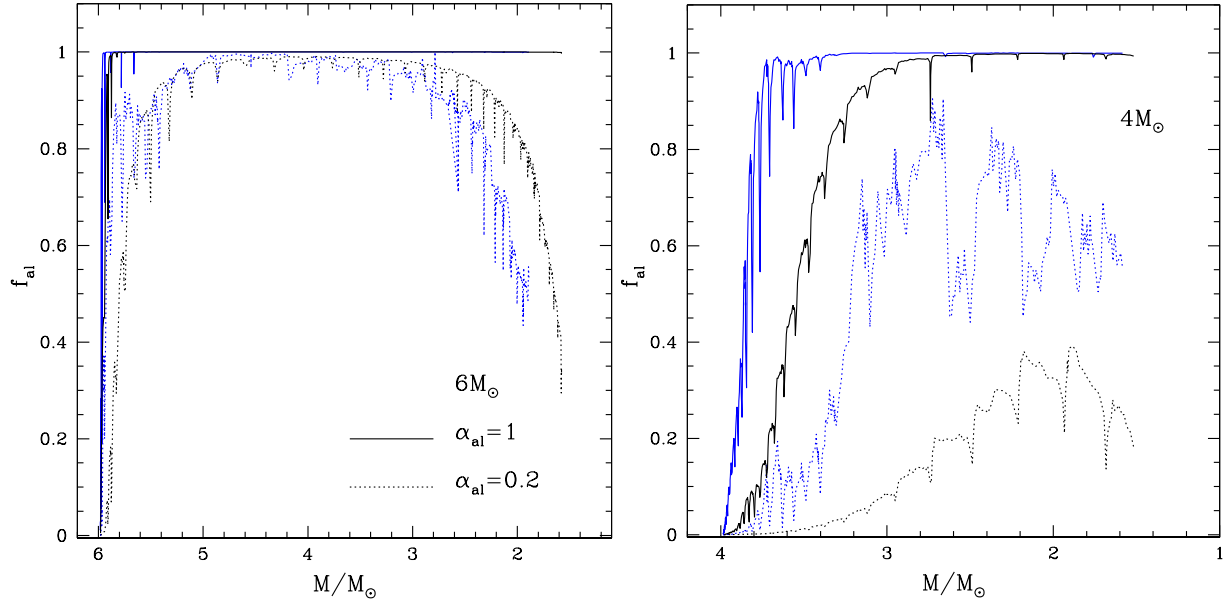


Figure 6. Evolution of the aluminium fraction condensed in Al_2O_3 (f_{al}) as a function of the evolution of the total mass for $6 M_{\odot}$ (left panel) and $4 M_{\odot}$ (right panel) initial mass model, at $Z = 0.004$ (black) and $Z = 0.018$ (blue). We explore $\alpha_{\text{al}} = 0.2$ (dotted line) and $\alpha_{\text{al}} = 1$ (solid lines) for both cases.

experienced by the Nanni et al. (2013) AGB models, where the lower mass ($< 5 M_{\odot}$) stars become C-rich, inhibiting the Al_2O_3 production.

5 COMPARISON WITH OBSERVATIONS

5.1 Al depletion in HBB AGB stars: a further indicator of Al_2O_3 dust production?

From the previous sections we know that formation of Al_2O_3 grains is favored by HBB conditions. In addition, the production of alumina dust implies an important decrease in the abundance of gaseous aluminium in the AGB wind. An important consequence of the high aluminium fraction condensed in Al_2O_3 that we find in our models (especially in the more massive AGB models) is that we predict gaseous Al to be underabundant in the more massive HBB AGB stars. Interestingly, McSaveney et al. (2007) found gaseous Al to be severely depleted (by almost one order of magnitude) in the HBB AGB star HV 2576 in the Large Magellanic Cloud (LMC)³. The surface chemistry of HV 2576 shows the imprinting of HBB, with a surface carbon content ~ 10 times smaller than expected, a small depletion of the surface oxygen, and a $+0.8$ dex increase in the nitrogen abundance. Because aluminium is not expected to undergo any destruction process in AGB stars (see left panel of Fig. 2), we interpret the strong Al depletion observed in HV 2576 as a further indicator for the formation of Al_2O_3 (which absorbs part of the gaseous aluminium available) in massive AGB stars.

³ Note that, to date, Al abundances have not been obtained in solar metallicity massive AGB stars.

Figure 8 shows the variation of the surface abundances of the CNO elements and of aluminium in models with metallicity $Z=0.008$ (appropriate for the LMC) and initial masses of 4, 5, and $6 M_{\odot}$. In the determination of the Al mass fraction, we subtract the amount of aluminium that is used to form Al_2O_3 . The thin horizontal lines in Figure 8 indicate the upper and lower value of the abundances observed in HV 2576. We note the signature of HBB in the three AGB models, with the depletion of the surface carbon in favour of nitrogen, together with a small reduction of the surface oxygen.

The analysis of the predicted carbon and nitrogen abundances are of little help in selecting the progenitor mass (and evolutionary status) of HV 2576; all models achieve the CN cycle in the external envelope, with the consequent destruction of the surface carbon by ~ 1 dex and the increase in the nitrogen content, both of them well within the observed range. The comparison between the observed and predicted oxygen abundances can be used only to rule out the possibility that HV 2576 is a massive AGB at the latest evolutionary stage. Contrary to the CNO elements, the aluminium content shows a greater variation with the initial stellar mass and the evolutionary status on the AGB. The extremely low gaseous Al abundance measured in HV 2576 demands a considerable production of alumina dust, which is only achieved for the $6 M_{\odot}$ model in the evolutionary phase of maximum Al_2O_3 production (i.e., well before the tip of the AGB). Thus, the Al abundance in HBB AGB stars turns out to be a good possible indicator of the progenitor mass and evolutionary status on the AGB.

The possible use of the Al content as a mass and/or evolutionary stage indicator in HBB AGB stars should be investigated in the future; e.g., the Al abundances could be

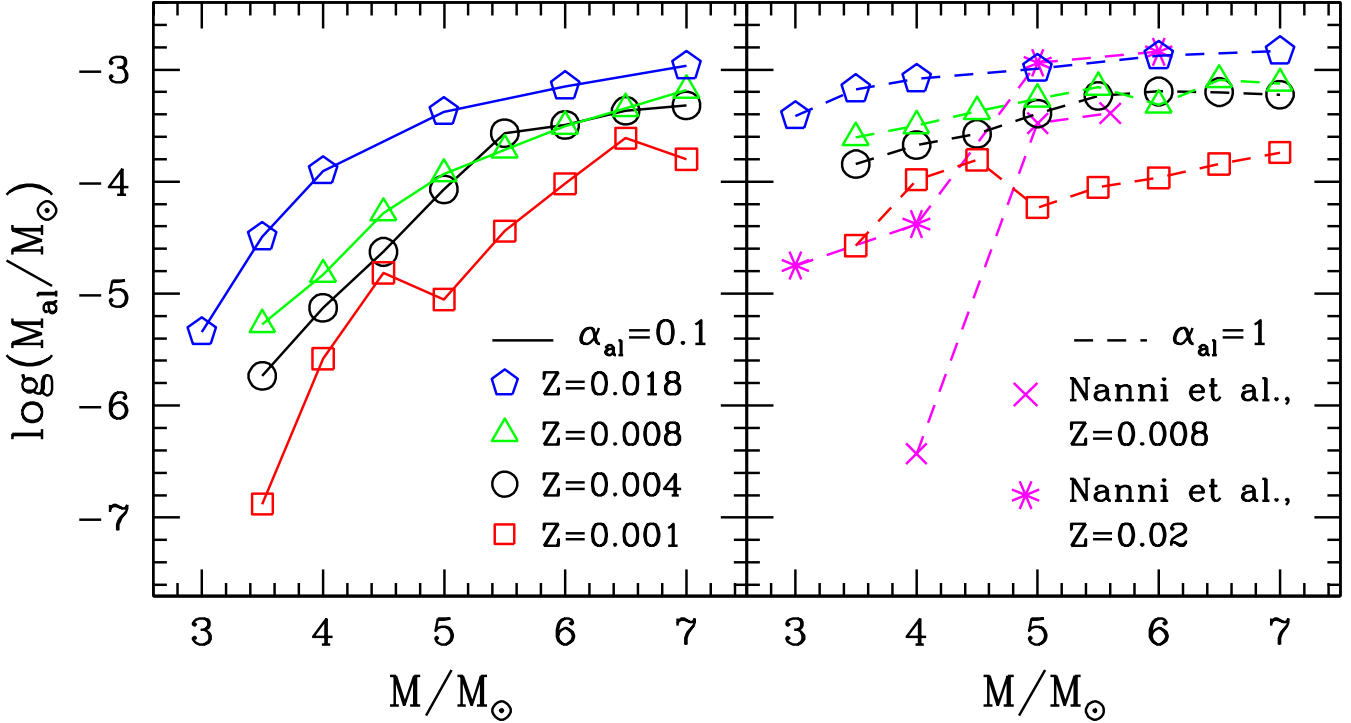


Figure 7. Alumina dust mass produced during the entire AGB phase as a function of the initial stellar mass at $Z = 0.001$ (red open squares), 0.004 (black open circles), 0.008 (green open triangles), and 0.018 (blue open pentagons). In the left panel, we show results obtained by assuming $\alpha_{\text{al}} = 0.1$ (solid line), while in the right panel α_{al} is 1 (dashed line). In the right panel, we also report results from Nanni et al. 2013, which consider $\alpha_{\text{al}} = 1$ at $Z = 0.008$ (magenta cross) and $Z = 0.02$ (magenta star)

measured in well known HBB AGB stars at different metallicities. Such direct comparisons of observed abundances and theoretical predictions will become more reliable once we completely understand the dust formation process and/or we know the Al_2O_3 sticking coefficient. However, from our comparison with HV 2576, it is clear how the theoretical description of the AGB phase, and particularly of the HBB phenomenon, can potentially benefit from the understanding of the Al_2O_3 dust formation process in stars experiencing HBB.

5.2 The Al_2O_3 dust condensation zone in Galactic O-rich AGB stars

A valuable test for our description of the alumina dust formation process in O-rich AGB stars is the comparison of our results with the recent findings by Karovicova et al. (2013). These authors have recently analyzed a small sample of three Galactic (i.e., solar metallicity) O-rich AGB stars (S Ori, R Cnc, and GX Mon) by means of spatially and spectrally resolved mid-infrared interferometric observations. Two stars (S Ori and R Cnc) in their sample are dominated by Al_2O_3 dust and the third one (GX Mon) displays a mix of Al_2O_3 and Mg-silicates. Indeed, their observations indicate that the inner radii of the Al_2O_3 shell for the three stars is located at a radial distance from the center of the star of $\sim 2 R_*$ (where R_* is the stellar radius), while Mg-silicates

are formed at larger radial distances. Taking into account all possible observational errors (e.g., the distances to these Galactic sources are very uncertain) as well as the uncertainties in the theoretical modelling (mass loss, sticking coefficient, etc.), these interferometric observations are in very good agreement (especially for Al_2O_3) with our model predictions for solar metallicity AGB stars (see Figure 3).

Indeed, in our AGB wind models, the region where Al_2O_3 forms gets closer the stellar surface as the AGB evolution proceeds. This is due to the decreasing trend of the effective temperature, which is rather similar for models of different progenitor mass. Independently of the initial mass, we find that Al_2O_3 formation initially begins at $\sim 2.5 R_*$, decreasing down to $\sim 1.5 R_*$ towards the end of the AGB phase. Unfortunately, our predicted radii for the Al_2O_3 dust condensation zone cannot be used to constrain the exact mass (and evolutionary status) of O-rich AGB stars but the observations ($\sim 2 R_*$) by Karovicova et al. (2013) lie just between our predicted range of ~ 1.5 - $2.5 R_*$ for the Al_2O_3 region and seem to support the reliability of our dust formation description.

Furthermore, Karovicova et al. (2013) found that the optical depth in the V-band for their sample stars is in the range $\tau_V \sim 1.3 - 2$. This fact could rule out the possibility of these stars being AGB stars with initial mass above $5 M_{\odot}$, because in our high-mass models the optical depth attains values $\tau_V > 4$ during the whole thermally pulsing phase.

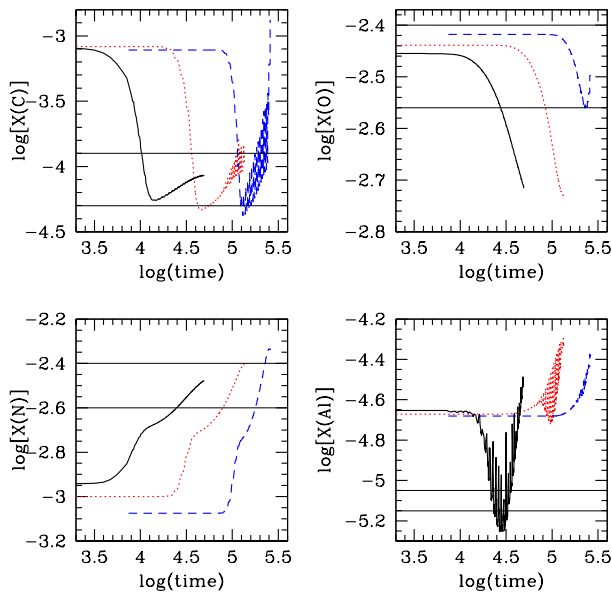


Figure 8. The variation with time (counted from the beginning of the AGB phase) of the surface abundances of carbon (top-left panel), nitrogen (bottom-left panel), oxygen (top-right panel) and aluminium (bottom-right panel) of stars with initial mass of 4 (blue dashed line), 5 (red dotted line), and 6 M_{\odot} (black solid line). The surface aluminium shown takes into account the amount of gaseous Al condensed into Al_2O_3 grains. The thin horizontal lines mark the limits of the abundances observed in the metal-poor HBB AGB star HV 2576 (McSaveney et al. 2007).

However, these stars could be the descendants of stars with initial mass between 4 and 5 solar masses; lower mass models achieve only a modest (if any) production of alumina dust, whereas stars more massive than $\sim 5 M_{\odot}$ evolve at optical depths much larger than observed by Karovicova et al. (2013). If the initial mass of the star is close to the lower limit of $\sim 4 M_{\odot}$ given above, we suggest that it is observed in an advanced AGB stage, e.g., after ~ 10 - 20 thermal pulses because τ_V is too small in the earlier AGB phases. Conversely, if the initial stellar mass is $\sim 5 M_{\odot}$, then we propose that the star is in the early AGB phase, because the optical depth becomes too large in more advanced evolutionary stages. Indeed, based on some observational properties (e.g., the characteristics of the maser emission, variability periods, infrared colors, etc.; see e.g., Garcia-Hernandez et al. 2006, 2007a), one could argue that GX Mon is more evolved and/or more massive than S Ori and R Cnc.

6 CONCLUSIONS

We investigate the production of alumina dust (Al_2O_3) in the circumstellar envelopes of O-rich AGB stars. We focused on those AGB stars experiencing HBB, with masses $M \geq 3M_{\odot}$. The range of metallicities examined is $10^{-3} \leq Z \leq 0.018$; lower metallicity stars are not expected to produce Al_2O_3 due to the extremely low Al abundance.

Al_2O_3 is the most stable oxygen-bearing dust species and its condensation process begins at temperatures $T \sim 1500$ K, which is considerably larger than that for Mg-

silicates ($T \sim 1100$ K) and iron ($T \sim 1000$ K). Thus, alumina dust grains form very close to the surface of the star, at radial distances from the stellar centre ranging from $\sim 2 R_*$ (for solar metallicity models) to $\sim 4 R_*$ (for $Z = 10^{-3}$). This result finds a robust confirmation in the recent interferometric observations of Galactic (i.e., solar metallicity) O-rich AGB stars by Karovicova et al. (2013).

The amount of Al_2O_3 formed scales almost linearly with the metallicity, owing to the larger surface abundances of aluminium in the higher metallicity models. The maximum production of alumina dust occurs in massive AGBs at solar metallicity, with a total Al_2O_3 mass of $\sim 10^{-3} M_{\odot}$. This sets an upper limit to the mass of Al_2O_3 that can be formed around AGB stars - in the higher metallicity models the Al_2O_3 formation process is so efficient that all the gaseous Al is absorbed and there is no possibility for further condensation. The Al_2O_3 grain size decreases with decreasing metallicity and progenitor mass. The maximum Al_2O_3 dust grain size of $\sim 0.075 \mu\text{m}$ (at solar metallicity) is considered as an upper limit to size of the alumina dust grains that can be formed around AGB stars.

The formation of alumina dust turns out to be extremely sensitive to the initial mass of the star. Models with $M < 5M_{\odot}$ experience soft HBB, and thus the condensation of gaseous Al-based molecules is less efficient. The masses of the Al_2O_3 dust formed around AGB stars of $\sim 3 - 4M_{\odot}$ is ~ 100 times smaller than that for their more massive counterparts.

The amount of gaseous Al available at the stellar surface severely decreases when alumina dust forms. Remarkably, this is consistent with the strong Al depletion seen in the low-metallicity HBB AGB star HV 2576. We suggest that the measurement of the Al abundances in HBB AGB stars could be potentially used as a proxy of the strength of HBB experienced by the star (e.g., stellar mass and evolutionary status).

Our conclusions - particularly for the predicted trend of the Al_2O_3 formed versus the initial stellar mass - are partly affected by the specific value of the sticking coefficient ($\alpha_{al}=0.1$, assumed to be similar to that of Mg-silicates), which gives the efficiency of the condensation process. For α_{al} values closer to unity, the Al_2O_3 formation as a function of the progenitor mass would be much flatter because the saturation conditions would occur even for $\sim 3 - 4M_{\odot}$ AGB stars.

ACKNOWLEDGMENTS

The authors are indebted to the referee, Aki Takigawa, for the careful reading of the manuscript and for the detailed and relevant comments, that helped to increase the quality of this work. D.A.G.H. acknowledges support provided by the Spanish Ministry of Economy and Competitiveness under grants AYA-2011-27754 and AYA-2011-29060. P.V. was supported by PRIN MIUR 2011 "The Chemical and Dynamical Evolution of the Milk Way and Local Group Galaxies" (PI: F. Matteucci), prot. 2010LY5N2T. R.S. acknowledges funding from the European Research Council under the European Union's Seventh Framework Programme (FP/2007-2013) / ERC Grant Agreement n. 306476.

REFERENCES

- Begemann B., Dorschner J., Henning Th., Mutschke H., Guertler J., Koempe C., Nass R., 1997, *ApJ*, 476, 199
- Bell K.R., Lin D.N.C., 1994, *ApJ*, 427, 987
- Blöcker T., 1995, *A&A*, 297, 727
- Blöcker T., Schönberner D., 1991, *A&A*, 244, L43
- Blommaert J. A. D. L., Groenewegen M. A. T., Okumura K., Ganesh S., Omont A., Cami J., Glass I. S., Habing H. J., Schultheis M., Simon G., van Loon J. Th., 2006, *A&A*, 460, 555
- Canuto V.M.C., Mazzitelli I., 1991, *ApJ*, 370, 295
- Cherchneff, I., & Cau, P. 1999, in *Proc. IAU Symp. 191, Asymptotic Giant Branch Stars*, ed. T. Le Bertre, A. Lebre, & C. Waelkens (San Francisco, CA:ASP), p. 251
- Choi B., Huss G. R., Wasserburg G. J., Gallino R., 1998, *Science*, 282, 1284
- DePew K., Speck A., Dijkstra C., 2006, *ApJ*, 640, 971
- Di Criscienzo M., Dell'Agli F., Ventura P., Schneider R., Valiante R., La Franca F., Rossi C., Gallerani S., Maiolino R., 2013, *MNRAS*, 433, 313
- Ferrarotti A.D., Gail H.P., 2001, *A&A*, 371, 133
- Ferrarotti A.D., Gail H.P., 2002, *A&A*, 382, 256
- Ferrarotti A.D., Gail H.P., 2006, *A&A*, 553, 576
- Gail H.P., Sedlmayr E., 1985, *A&A*, 148, 183
- Gail H.P., Sedlmayr E., 1998, *Faraday Discussions*, 109, 303
- Gail H.P., Sedlmayr E., 1999, *A&A*, 347, 594
- Gall C., Hjorth J., Andersen A. C., 2011, *A&ARv*, 19, 43
- García-Hernández D. A., García-Lario, P., Plez, B. et al. 2006, *Science*, 314, 1751
- García-Hernández D. A., García-Lario, P., Plez, B. et al. 2007a, *A&A*, 462, 711
- García-Hernández D. A., Perea-Calderón, J. V., Bobrowsky, M., García-Lario, P. 2007b, *ApJ*, 666, L33
- García-Hernández D. A., García-Lario, P., Plez, B. et al. 2009, *ApJ*, 705, L31
- García-Hernández, D. A., Zamora, O., Yagüe, A. et al. 2013, *A&A*, 555, L3
- Gomez H. L. et al., 2012, *MNRAS*, 420, 3557
- Grevesse N., Sauval A.J., 1998, *SSrv*, 85, 161
- Herwig F., 2005, *AR&A*, 43, 435
- Hutcheon I. D., Huss G. R., Fahey A. J., Wasserburg G. J., *ApJL*, 425, 97
- Jones O. C., Kemper F., Srinivasan S., McDonald I., Sloan G. C., Zijlstra A. A., 2014, *arXiv:1402.2485*
- Karovicova, I., Wittkowski, M., Ohnaka, K. et al. 2013, *A&A* (in press; *arXiv:1310.1924*)
- Knapp G. R., 1985, *ApJ*, 293, 273
- Koike C., Kaito C., Yamamoto T., Shibai H., Kimura S., Suto H., 1995, *Icarus*, 114, 203
- Levin V., Brandon M., 1998, *J.Am.Ceram.Soc.*, 81, 1995
- Lugaro M., Doherty C. L., Karakas A. I., Maddison S. T., Liffman K., García-Hernández D. A., Siess L., Lattanzio J. C., 2012, *M&PS*, 47, 1998
- Lorenz-Martins, S., & Pompeia, L. 2000, *MNRAS*, 315, 856
- McSaveney, J. A., Wood, P. R., Scholz, M. et al. 2007, *MNRAS*, 378, 1089
- Maldoni, M. M., Ireland, T. R., Smith, R. G., Robinson, G. 2005, *MNRAS*, 362, 782
- Matsuura M., Dwek E., Meixner M., et al. 2011, *Science*, 333, 1258
- Mazzitelli I., D'Antona F., & Ventura P. 1999, *A&A*, 348, 846
- Nanni A., Bressan A., Marigo P., Girardi L. 2013, *MNRAS*, 434, 2390
- Nittler L. R., Alexander C. M. O., Gallino R., Hoppe P., Nguyen A. N., Stadermann F. J., Zinner E. K., 2008, *ApJ*, 682, 1450
- Norris, B. R. M., Tuthill P. G., Ireland M. J. et al. 2012, *Nature*, 484, 220
- Kerschbaum F., Mutschke H., Fabian D., Dorschner J., Hron J., 1999, *A&A*, 352, 609
- Renzini A., Voli M., 1981, *A&A*, 94, 175
- Schwarzschild M., Harm R., 1965, *ApJ*, 142, 855
- Schwarzschild M., Harm R., 1967, *ApJ*, 145, 496
- Sedlmayr E., 1989, *Interstellar Dust: Proceedings of the 135th Symposium of the International Astronomical Union, held in Santa Clara, California, 26-30 July 1988*. Edited by Louis J. Allamandola and A. G. G. M. Tielens. International Astronomical Union.
- Sharp C. M., Huebner W. F., 1990, *Astrophysical Journal Supplement Series*, 72, 417
- Sloan G. C., Kraemer Kathleen E., Goebel J. H., Price Stephan D., 2003, *ApJ*, 584, 493
- Sylvester, R. J., Kemper, F., Barlow, M. J. et al. 1999, *A&A*, 352, 587
- Takigawa A., Tachibana S., Nagahara H., Ozawa K., 2009, 40th Lunar and Planetary Science Conference, held March 23-27, 2009 in The Woodlands, Texas, id.1731
- Takigawa A., Tachibana S., Nagahara H., Ozawa K., 2012, 43rd Lunar and Planetary Science Conference, 2012, 1875
- Takigawa A., Tachibana S., Huss G. R., Nagashima K., Makide K., Krot A. N., Nagahara H., 2014, *GCA*, 124, 309
- Tenorio-Tagle, G., Silich, S., Martínez-González, S. et al. 2013, *ApJ*, 778, 159
- Tielens, A. G. G. M., Waters, L. B. F. M., Molster, F. J., & Justtanont, K. 1998, *Ap&SS*, 255, 415
- Trigo-Rodríguez, J. M., García-Hernández, D. A., Lugaro, M. et al. 2009, *M&PS*, 44, 627
- Valiante R., Schneider R., Bianchi S., Andersen A., Anja C., 2009, *MNRAS*, 397, 1661
- Ventura P., Carini R., D'Antona F., 2011, *MNRAS*, 415, 3865
- Ventura P., Di Criscienzo M., Carini R., D'Antona F., 2013, *MNRAS*, 431, 3642
- Ventura P., D'Antona F., 2005, *A&A*, 341, 279
- Ventura P., D'Antona F., 2009, *A&A*, 499, 835
- Ventura P., Di Criscienzo M., Schneider R., Carini R., Valiante R., D'Antona F., Gallerani S., Maiolino R., Tornambé A., 2012a, *MNRAS*, 420, 1442
- Ventura P., Di Criscienzo M., Schneider R., Carini R., Valiante R., D'Antona F., Gallerani S., Maiolino R., Tornambé A., 2012b, *MNRAS*, 424, 2345
- Ventura P., Dell'Agli F., Di Criscienzo M., Schneider R., Rossi C., La Franca F., Gallerani S., Valiante R., 2014, *arXiv:1401.1332*
- Ventura P., Zeppieri A., Mazzitelli I., D'Antona F., 1998, *A&A*, 334, 953
- Wachter A., Winters J. M., SchrSchrderAder K. P., Sedlmayr E., 2008, *A&A*, 486, 497
- Woitke P., 2006, *A&A*, 460, L9
- Yang X., , Chen, P., & He, J. 2004, *A&A*, 414, 1049
- Yang X., 2008, *New Astronomy*, 13, 593

Zhao-Geisler R., Quirrenbach A., Köhler R., Lopez B.,
2012, A&A, 545, A56
Zeidler S., Posch Th., Mutschke H., 2013, A&A, 553, A81